IOP Publishing Journal of Geophysics and Engineering
J. Geophys. Eng. 15 (2018) 995–1007 (13pp) https://doi.org/10.1088/1742-2140/aa8cb6

Seismic instantaneous frequency extraction based on the SST-MAW

Naihao Liu[1], Jinghuai Gao[1,5], Xiudi Jiang[2], Zhuosheng Zhang[3] and Ping Wang[4]

[1] School of Electronic and Information Engineering, Xi'an Jiaotong University and National Engineering Laboratory for Offshore Oil Exploration, Xi'an, 710049, People's Republic of China
[2] Geophysics Key Lab, Technology R&D Center, Research Institute of China National Offshore Oil Corporation (CNOOC) and National Engineering Laboratory for Offshore Oil Exploration, Beijing, 100029, People's Republic of China
[3] School of Mathematics and Statistics, Xi'an Jiaotong University, Xi'an, 710049, People's Republic of China
[4] Xi'an Institute of Space Radio Technology, Xi'an, 710100, People's Republic of China

E-mail: lnhfly@163.com, jhgao@mail.xjtu.edu.cn, jiangxd2@cnooc.com.cn, zszhang@mail.xjtu.edu.cn and 120966868@qq.com

Received 13 January 2017, revised 23 August 2017
Accepted for publication 14 September 2017
Published 13 March 2018

Abstract

The instantaneous frequency (IF) extraction of seismic data has been widely applied to seismic exploration for decades, such as detecting seismic absorption and characterizing depositional thicknesses. Based on the complex-trace analysis, the Hilbert transform (HT) can extract the IF directly, which is a traditional method and susceptible to noise. In this paper, a robust approach based on the synchrosqueezing transform (SST) is proposed to extract the IF from seismic data. In this process, a novel analytical wavelet is developed and chosen as the basic wavelet, which is called the modified analytical wavelet (MAW) and comes from the three parameter wavelet. After transforming the seismic signal into a sparse time–frequency domain via the SST taking the MAW (SST-MAW), an adaptive threshold is introduced to improve the noise immunity and accuracy of the IF extraction in a noisy environment. Note that the SST-MAW reconstructs a complex trace to extract seismic IF. To demonstrate the effectiveness of the proposed method, we apply the SST-MAW to synthetic data and field seismic data. Numerical experiments suggest that the proposed procedure yields the higher resolution and the better anti-noise performance compared to the conventional IF extraction methods based on the HT method and continuous wavelet transform. Moreover, geological features (such as the channels) are well characterized, which is insightful for further oil/gas reservoir identification.

Keywords: seismic instantaneous frequency, synchrosqueezing, noise immunity, analytic signal

(Some figures may appear in colour only in the online journal)

1. Introduction

Instantaneous attributes extracted from seismic data are widely applied in identifying abnormal attenuation, detecting faults in stratigraphy, and seismic stratigraphic interpretation (Chopra and Marfurt 2005). Complex seismic trace attributes are one of the most commonly used post-stack attributes, which are derived from complex-trace analysis (Taner *et al* 1979). These attributes include instantaneous amplitude, instantaneous frequency (IF), instantaneous phase, instantaneous bandwidth, etc. As one of the most commonly used attributes, IF is successfully applied to sub-surface structural analysis, thin-bed tuning, quality factor (Q) inversion, and boundaries characterization of different fluid saturated rocks (Chopra and Marfurt 2005, Huang and Wu 2008, Yang and Gao 2010, Kourki and Riahi 2014). Although IF has been

[5] Author to whom any correspondence should be addressed.

applied to seismic exploration for several decades, improving the estimation precision and the anti-noise performance are still challenges (Barnes 1993, Guo *et al* 2008).

In general, seismic IF extraction based on complex-trace analysis is divided into two categories: Hilbert transform (HT) based methods and time–frequency transform based approaches (such as continuous wavelet transform (CWT), and windowed Fourier transform, etc). The HT based IF extraction, was introduced by Taner *et al* (1979) and has been widely applied to seismic data interpretation (Barnes 1993, 2007). The seismic trace is treated as the real part of the analytical signal, while the corresponding imaginary part is computed by taking the HT of the seismic trace (Chopra and Marfurt 2005). Taner *et al* (1979) introduced seismic IF extraction to the industry and developed a single mathematical framework for attribute computation. Marfurt *et al* (1998) generalized the calculation of conventional complex trace attribute to the calculation of complex reflector attributes. Moreover, he combined these attributes with coherency and dip/azimuth cubes to provide a multi-attribute analysis. Guo *et al* (2008) stated that proper scaling, attribute choice, and color models can provide a means to rapidly scan large volumes of seismic data to identify geologic features. Fomel (2007) introduced the concept of local seismic attributes, which measure signal characteristics in the neighborhood of each point. Wang *et al* (2013) proposed a fractional IF extraction technique using the Caputo operator and showed the interpretive value of an anomalous IF to characterize a sandstone channel. However, the estimated IF based on the HT method will degrade in a noisy environment because the differentials enhance noise during its calculation. The noise in seismic signals makes it difficult to get an accurate and effective calculation of the IF and interpret the geological structure of the subsurface, especially in a low signal to noise ratio (SNR) environment.

Another IF extraction methods, based on complex-trace analysis, are time–frequency analysis based, which can overcome the noise sensitivity (Gao *et al* 1999, Barnes 2007, Li *et al* 2014). Zoukaneri and Porsani (2015) devised a formula to estimate a robust and stable average IF in the time domain by combining the Wigner–Ville distribution and the maximum entropy method of Burg (1975). Among various time–frequency transform tools, the CWT is frequently used to estimate IF, because the subsequent signal reconstruction using a basic analytical wavelet represents the corresponding analytic signal of the input real-valued seismic signal (Gao *et al* 1999). Gao *et al* (1999) proposed IF extraction by taking advantage of the CWT and produced a robust IF estimation. Wang and Gao (2013) introduced the generalized Morse wavelet (Olhede and Walden 2002, Lilly and Olhede 2012) to estimate the IF based on the CWT, which can constitute a tighter frame than the Morlet wavelet family. This provides a sparser time–frequency representation and a simple means of recovering the original signal from its frame coefficients. The energy distribution of the effective signal is confined in a small subspace of the time-scale domain (Wang and Gao 2013), while that of the noise may be dispersed in a larger subspace (even over the whole time-scale domain) with a lower amplitude. Based on this concept, the adaptive threshold strategy (Donoho 1995, Herrera *et al* 2014) suppresses noise in the time-scale domain. Thus, wavelet-based IF estimation methods can yield more stable and accurate results compared to the HT based approaches. Although the IF extracted by the wavelet-based method shows good anti-noise performance, its resolution needs further improvement to distinguish small geological structures. Because of the Heisenberg uncertainty principle limiting time–frequency resolution, energy spreads out over the time–frequency plane. Different trade-offs can be achieved by the choice of the linear transform or the generators for the family of templates, but none is ideal, thereby causing a negative impact on time–frequency domain denoising and IF estimation, especially in a low SNR environment.

The synchrosqueezing transform (SST) proposed by Daubechies *et al* (2011) provides an alternative method of obtaining a high time–frequency resolution by means of reallocating coefficients of the time–frequency plane along the frequency axis (Wang *et al* 2014). This transform can also accurately reconstruct the input signal. In this study, we take advantage of this transform and propose a novel approach based on the SST (Daubechies *et al* 2011, Brevdo *et al* 2013) to extract seismic IF. This transform can preferably identify the frequency distribution of seismic signals. Based on the three parameter wavelet (TPW), we develop a novel wavelet and choose it as the basic wavelet in the SST, which is called the modified analytical wavelet (MAW). The MAW is an exact analytic wavelet and able to match different seismic wavelets better when compared with other common wavelets (such as the Morlet wavelet) used in the seismic signal analysis (Gao *et al* 2006). The experimental results indicate that the proposed IF extraction approach shows a significant improvement in comparisons with classical methods, especially for anti-noise performance and high resolution.

This paper is organized as follows. First, the conventional complex-trace analysis methods based on the HT and the CWT are briefly introduced. Second, some basic facts concerning the SST and the MAW are reviewed. Then, the seismic IF extraction based on the SST taking the MAW (SST-MAW) is proposed in detail. Finally, synthetic data and field seismic data experiments are presented. Detailed discussions and conclusions end this paper.

2. Instantaneous frequency extraction via the HT and CWT based methods

For a real-valued signal $s(t)$, the definition of the corresponding analytic signal $z(t)$ is (Taner *et al* 1979)

$$z(t) = s(t) + \mathrm{i}h(t), \tag{1}$$

where the imaginary part $h(t)$ denotes the HT of $s(t)$. Then, the IF exacted by the HT approach can be defined as

$$f(t) = \frac{1}{2\pi}\frac{\mathrm{d}}{\mathrm{d}t}\left[\arctan\left[\frac{h(t)}{s(t)}\right]\right] = \frac{1}{2\pi}\frac{s(t)h'(t) - s'(t)h(t)}{e^2(t)}, \tag{2}$$

where $e^2(t) = s^2(t) + h^2(t)$. The estimated IF result degrades in a noisy environment due to the differential, which enhances noise in the calculation of the IF. Large spikes in the IF calculation occur in a noisy environment when the denominator of equation (2) approaches to zero more rapidly than the numerator. To eliminate the impact of the noise and avoid division by zero, Gao *et al* (1999) suggested introducing a damping coefficient ε in equation (2).

$$f(t) = \frac{1}{2\pi}\frac{s(t)h'(t) - s'(t)h(t)}{e^2(t) + \varepsilon e^2{}_{\max}}, \tag{3}$$

where $0 < \varepsilon < 1$ and $e_{\max} = \max(e(t))$. Many estimation methods are based on equation (3). For simplicity, we choose the damping coefficient as 0.05 in this paper. Even with the damping, this IF estimation method is still sensitive to noise on account of the presence of differential operations.

The CWT based method is another complex-trace analysis method. For a given signal $s(t) \in L^2(R, \mathrm{d}t)$ with the basic wavelet $\psi(t)$, the CWT is defined as

$$S_s(b, a) = \int_{-\infty}^{\infty} a^{-1}s(t)\overline{\psi\left(\frac{t-b}{a}\right)}\mathrm{d}t, \tag{4}$$

where $t, b \in R$, R is the real number set, a represents the scale, $a > 0$, and $\overline{\psi(t)}$ is the complex conjugate of $\psi(t)$. Because it is more convenient for oscillatory signals (Lilly and Olhede 2010), the normalization factor is chosen to be $1/a$ instead of the more common $1/\sqrt{a}$. The wavelet should satisfy the admissibility condition (Holschneider and Kon 1996):

$$C_\psi = \int_{-\infty}^{\infty} |\hat{\psi}(\omega)|/|\omega|\ \mathrm{d}\omega < \infty, \tag{5}$$

where $\hat{\psi}(\omega) = \int_{-\infty}^{\infty} \psi(t)\mathrm{e}^{-\mathrm{i}\omega t}\mathrm{d}t$ is the Fourier transform of the basic wavelet. If the input signal is noisy of unknown level, the threshold ς of Herrera *et al* (2014) is used to suppress noise as given by

$$\varsigma = \sqrt{2\log_2 N}\cdot\sigma_\eta, \tag{6}$$

where $\sigma_\eta = \mathrm{median}(|S_s(a_{1:n_v}, b) - \mathrm{median}(S_s(a_{1:n_v}, b))|)/0.6745$, $S_s(a_{1:n_v}, b)$ are the finest scale wavelet coefficients (Donoho 1995), N is the signal length and 0.6745 is the median absolute deviation of a Gaussian distribution.

Supposing an analytic wavelet chosen as the basic wavelet, Gao *et al* (1999) proved that

$$s(b) + \mathrm{i}H[s(b)] = \frac{1}{C_\psi}\int_0^{\infty} \mathrm{d}aS_s(a, b)a^{-1}, \tag{7}$$

where $H[s(b)]$ is the HT of $s(b)$. The IF of a real-valued seismic signal can be calculated with the reconstructed signal of the CWT, taking the place of the HT method via (3). For the CWT extraction described in this paper, the Morlet wavelet is chosen as the basic wavelet without the specified requirement.

3. Instantaneous frequency extraction via the SST-MAW

Based on the SST and the MAW, a novel method of extracting seismic IF is proposed in this paper, which is entitled the SST using the MAW (SST-MAW). The algorithmic procedure of the IF extraction, based on the SST-MAW, is detailed in this subsection.

It is well known that the result of the wavelet analysis is highly correlated to the choice of basic wavelet (Gao *et al* 1996, Torrence and Compo 1998, Harrop *et al* 2002). However, the TPW can provide an adjustable and optimizing temporal-frequency resolution (Gao *et al* 2006), because the three parameters can be modulated to different seismic waves. Therefore, choosing it as the basic wavelet can represent the seismic signal in time–frequency domain sparsely. It is also able to contribute to identifying the energy distribution of the effective seismic data. This approximate analytic wavelet in frequency domain is defined as follows

$$\begin{aligned}\psi(\omega;\ \Lambda) = &\sqrt{\frac{\pi}{\tau}}\frac{p(\Lambda) + q(\Lambda)}{2}\mathrm{e}^{-\mathrm{i}\beta(\omega-\sigma)-\frac{(\omega-\sigma)^2}{4\tau}}\\ &+ \sqrt{\frac{\pi}{\tau}}\frac{p(\Lambda) - q(\Lambda)}{2}\mathrm{e}^{-\mathrm{i}\beta(\omega+\sigma)-\frac{(\omega+\sigma)^2}{4\tau}}\\ &- \sqrt{\frac{\pi}{\tau}}p(\Lambda)k(\Lambda)\mathrm{e}^{-\mathrm{i}\beta\omega-\frac{\omega^2}{4\tau}}.\end{aligned} \tag{8}$$

Here,

$$\begin{aligned}k(\Lambda) &= \mathrm{e}^{-\frac{\sigma^2}{4\tau}}\left[\cos(\beta\sigma) + \mathrm{i}\frac{q(\Lambda)}{p(\Lambda)}\sin(\beta\sigma)\right],\\ p(\Lambda) &= \left(\frac{2\tau}{\pi}\right)^{\frac{1}{4}}[4(\mathrm{e}^{-\frac{\sigma^2}{2\tau}} - \mathrm{e}^{-\frac{3\sigma^2}{8\tau}}) \times \cos^2(\beta\sigma)\\ &\quad + 1 - \mathrm{e}^{-\frac{\sigma^2}{2\tau}}]^{-\frac{1}{2}},\\ q(\Lambda) &= \left(\frac{2\tau}{\pi}\right)^{\frac{1}{4}}[4(\mathrm{e}^{-\frac{\sigma^2}{2\tau}} - \mathrm{e}^{-\frac{3\sigma^2}{8\tau}}) \times \sin^2(\beta\sigma)\\ &\quad + 1 - \mathrm{e}^{-\frac{\sigma^2}{2\tau}}]^{-\frac{1}{2}},\end{aligned} \tag{9}$$

where σ denotes the modulated frequency, τ denotes the energy decay factor, β denotes the energy delay factor and $\Lambda = (\sigma, \tau, \beta)$ represents the set of σ, τ and β. These three parameters in such a wavelet can be adjusted; for example, choosing a smaller σ for a higher time resolution. When choosing $\sigma > 5.33$, the TPW is the same as the common Morlet wavelet. The energy decay factor τ, which controls the frequency bandwidth of TPW, is chosen smaller than 0.5 to get an approximate analytic basic wavelet. $\beta = 0$ is chosen to obtain a symmetrical basic wavelet in this paper, especially in the frequency domain. So the TPW in equations (8) and (9) can be rewritten for convenience as

$$\begin{aligned}\psi(\omega;\ \Lambda') = &\sqrt{\frac{\pi}{\tau}}\frac{p(\Lambda') + q(\Lambda')}{2}\mathrm{e}^{-\frac{(\omega-\sigma)^2}{4\tau}}\\ &+ \sqrt{\frac{\pi}{\tau}}\frac{p(\Lambda') - q(\Lambda')}{2}\mathrm{e}^{-\frac{(\omega+\sigma)^2}{4\tau}}\\ &- \sqrt{\frac{\pi}{\tau}}p(\Lambda')k(\Lambda')\mathrm{e}^{-\frac{\omega^2}{4\tau}},\end{aligned} \tag{10}$$

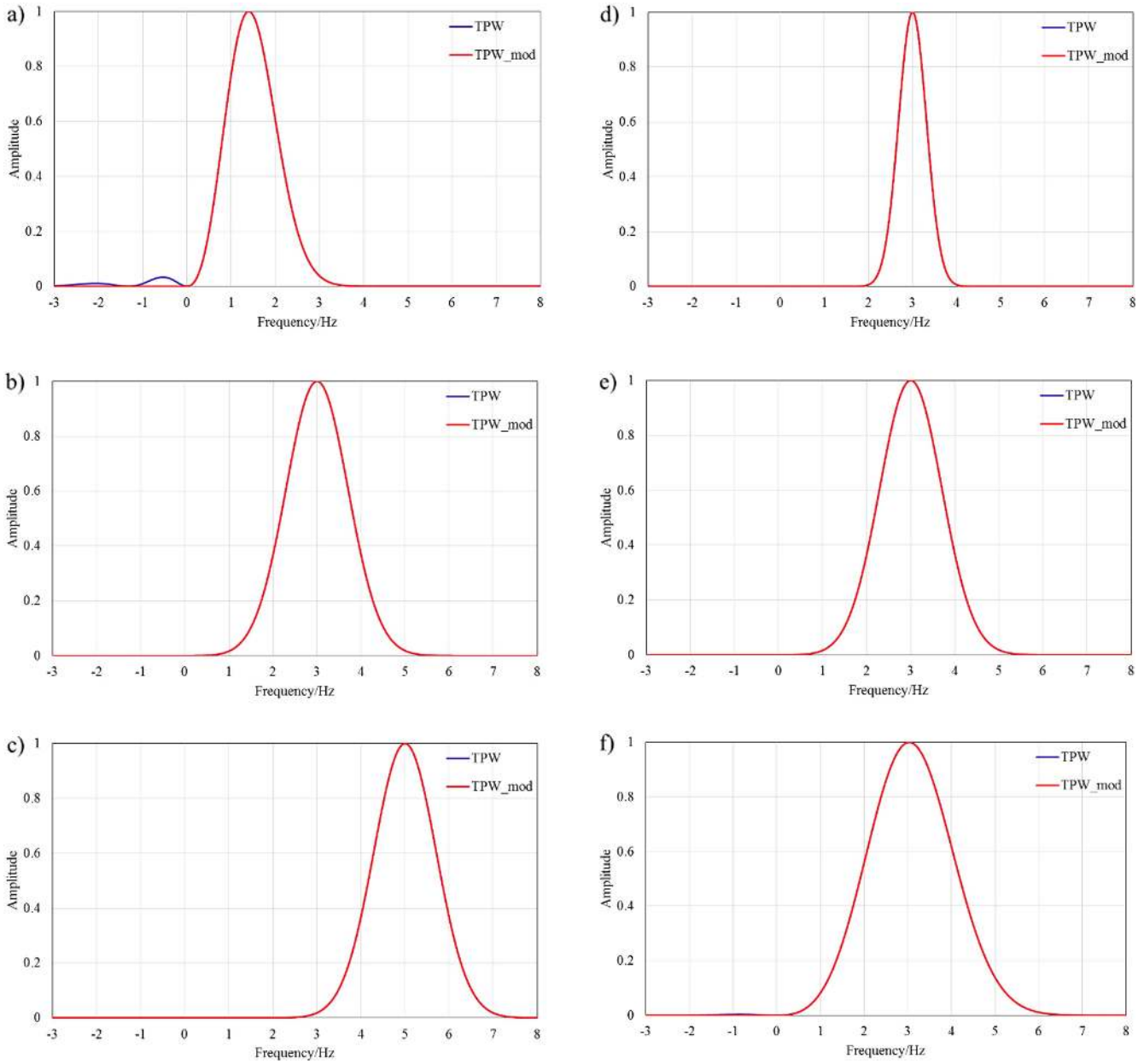

Figure 1. The TPW (in blue) and the MAW (in red) in the frequency domain. The TPW and MAW with (a) $\Lambda = (1,\ 0.5,\ 0)$, (b) $\Lambda = (3,\ 0.5,\ 0)$, (c) $\Lambda = (5,\ 0.5,\ 0)$, (d) $\Lambda = (3,\ 0.1,\ 0)$, (e) $\Lambda = (3,\ 0.5,\ 0)$, and (f) $\Lambda = (3,\ 1,\ 0)$.

$$k(\Lambda') = \mathrm{e}^{-\frac{\sigma^2}{4\tau}},$$
$$p(\Lambda') = \left(\frac{2\tau}{\pi}\right)^{\frac{1}{4}}\left[4\left(\mathrm{e}^{-\frac{\sigma^2}{2\tau}} - \mathrm{e}^{-\frac{3\sigma^2}{8\tau}}\right) + 1 - \mathrm{e}^{-\frac{\sigma^2}{2\tau}}\right]^{-\frac{1}{2}},$$
$$q(\Lambda') = \left(\frac{2\tau}{\pi}\right)^{\frac{1}{4}}\left[1 - \mathrm{e}^{-\frac{\sigma^2}{2\tau}}\right]^{-\frac{1}{2}}, \tag{11}$$

where $\Lambda' = (\sigma,\ \tau)$ represents the set of σ and τ. We need an analytic wavelet in the CWT in this paper, which will be explained in the following part. So we develop a MAW using equations (10) and (11), shown in equation (12).

$$\psi_{\mathrm{mod}}(\omega;\ \Lambda') = \psi(\omega;\ \Lambda')U(\omega), \tag{12}$$

where $U(\omega)$ is the Heaviside function and $\Lambda' = (\sigma,\ \tau)$. $\psi_{\mathrm{mod}}(\omega;\ \Lambda')$ is the MAW used in this paper, which is an analytical wavelet. The spectra of the TPW (in blue) and MAW (in red) are shown in figure 1 with regards to various parameters. It can be easily seen that the proposed MAW is an exact analytical wavelet, while the TPW is an appropriate one. Note the narrow window width in the frequency domain by choosing a small τ, which leads to an improved and adjustable time–frequency resolution using the MAW in the CWT.

As mentioned above, introducing this modified wavelet to time–frequency analysis of seismic signals can provide an adjustable and sparse time–frequency representation. Note

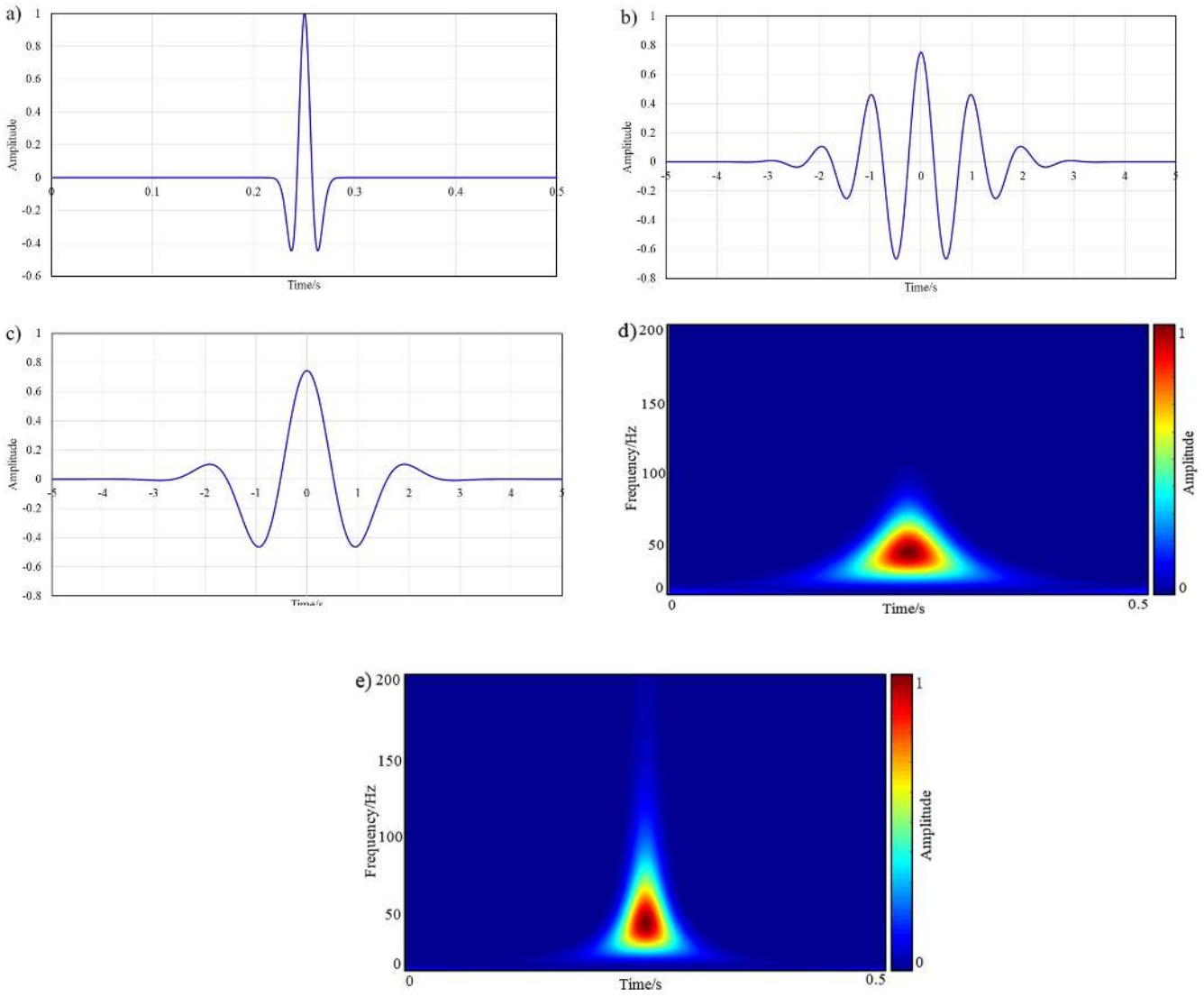

Figure 2. The Ricker wavelet example. (a) The test Ricker wavelet whose dominant frequency is 50 Hz, (b) and (c) denote the Morlet wavelet and MAW with $\Lambda = (3,\ 0.5)$, (d) and (e) represent the corresponding CWT representations based on the Morlet wavelet and MAW.

that how to choose appropriate parameters of the MAW is explained in detail in appendix A. A test example is provided in figure 2. The test signal is a Ricker wavelet, whose dominant frequency is 50 Hz. The Morlet wavelet and MAW with $\Lambda' = (3,\ 0.5)$ are shown in figures 2(b) and (c). Figures 2(d) and (e) represent the corresponding CWT representations using these two basic wavelets. Note that the CWT-MAW can get a higher time resolution than that using the Morlet wavelet because the MAW matches the Ricker wavelet better than the Morlet wavelet.

After reviewing the CWT in (4), we rewrite $S(b, a)$ by the Plancherel's theorem as

$$S(b,\ a) = \frac{1}{2\pi}\int_{-\infty}^{\infty} a^{-1/2}\hat{s}(\xi)\overline{\hat{\psi}_{\mathrm{mod}}(a\xi;\ \Lambda')}\mathrm{e}^{\mathrm{i}b\xi}\mathrm{d}\xi, \qquad (13)$$

where ξ is the angular frequency and $\hat{\psi}_{\mathrm{mod}}(\xi;\ \Lambda')$ is the Fourier transform of the MAW. Considering a simple case of a single harmonic signal $s(t) = A\cos(\omega t)$ whose Fourier transform is $\hat{s}(\xi) = \pi A[\delta(\xi - \omega) + \delta(\xi + \omega)]$, (13) can be rewritten as

$$\begin{aligned} S(b,\ a) &= \frac{A}{2}\int_{-\infty}^{\infty} a^{-1/2}[\delta(\xi - \omega) + \delta(\xi + \omega)] \\ &\quad \times \overline{\hat{\psi}_{\mathrm{mod}}(a\xi;\ \Lambda')}\mathrm{e}^{\mathrm{i}b\xi}\mathrm{d}\xi, \\ &= \frac{A}{2}a^{-1/2}\overline{\hat{\psi}_{\mathrm{mod}}(a\omega;\ \Lambda')}\,\mathrm{e}^{\mathrm{i}b\omega}. \end{aligned} \qquad (14)$$

If $\hat{\psi}_{\mathrm{mod}}(\omega;\ \Lambda')$ is concentrated around its central frequency $\xi = \omega_0$, then $S(b,\ a)$ will be concentrated around $a = \omega_0/\omega$. However, the wavelet transform $S(b,\ a)$ will be spread out over a region around the scale axis $a = \omega_0/\omega$, leading to a blurred result in the time-scale plane.

To reduce the influence of the spreading along the scale axis a after the CWT calculation using the MAW, a candidate

frequency $\omega_s(a, b)$ for the signal $s(t)$ (Daubechies *et al* 2011, Brevdo *et al* 2013) is introduced. $\omega_s(a, b)$ is computed with the CWT coefficients of (4) and (13) by

$$\omega_s(a, b) = \frac{\partial S_s(a, b)}{\partial b} \Big/ (\mathrm{i}S_s(a, b)), \tag{15}$$

where $S_s(a, b) \neq 0$ for any (a, b). A sufficiently small parameter ς is chosen as the threshold (Daubechies *et al* 2011, Wang *et al* 2014) such that $|S_s(a, b)| > \varsigma$. ς is chosen as 10^{-8} in the numerical implementation with higher SNR. When the noise level is unknown, the adaptive parameter in (6) is introduced as the threshold ς.

After the candidate frequency computation, the information from the time-scale domain can be transformed to the time–frequency domain, according to the map $(b, a) \rightarrow (b, \omega_s(a, b))$ (Daubechies *et al* 2011, Brevdo *et al* 2013). By summing different contributions, $T_s(\omega, b)$ can be calculated as

$$T_s(\omega_l, b) = \frac{1}{\Delta\omega} \sum_A S_s(a_k, b) a_k^{-1} (\Delta a)_k, \tag{16}$$

where $A = \{a_k: |\omega(a_k, b) - \omega_l| \leqslant \Delta\omega/2\}$. Note $a_k = 2^{k/n_v}\Delta t$, $k = 0, 1, \cdots, Ln_v - 1$, and Δt is the time sampling interval. n_v is chosen as 32 in the experiments. The time–frequency representation $T_s(\omega, b)$ is likewise determined only at the centers ω_l of the successive bins $[\omega_l - \Delta\omega/2, \omega_l + \Delta\omega/2]$, with $\omega_l - \omega_{l-1} = \Delta\omega$. The maximum frequency is $\omega_{\max} = \frac{1}{2\Delta t}$ and the minimum is $\omega_{\min} = \frac{1}{T} = \frac{1}{n\Delta t}$, where $T = n\Delta t$ is the signal duration. After collecting the time–frequency coefficients along the frequency axis, a sparse time–frequency representation is obtained (Wang and Gao 2013). After combining with the adaptive parameter ς as the threshold, the energy distribution of the effective seismic signal can be extracted accurately as

$$T_s(\omega_l, b) = \begin{cases} T_s(\omega_l, b) - \varsigma \dfrac{T_s(\omega_l, b)}{|T_s(\omega_l, b)|}, & |T_s(\omega_l, b)| \geqslant \varsigma \\ 0, & |T_s(\omega_l, b)| < \varsigma. \end{cases} \tag{17}$$

The original signal can still be reconstructed from the sparse time–frequency result in (17). When the MAW $\psi_{\mathrm{mod}}(t; \Lambda')$ is an analytic wavelet function with its real part being even and $\psi_{\mathrm{mod}}(t; \Lambda')$ satisfying the admissibility condition denoted in (5), and an arbitrary real $s(t) \in L^2(R, \mathrm{d}t)$ is given, we have

$$s(b) + \mathrm{i}H[s(b)] = \frac{1}{C_\psi} \sum_{l,\Omega} T_s(\omega_l, b)(\Delta\omega), \tag{18}$$

where $T_s(\omega_l, b)$ is defined as (17) and $H[s(b)]$ is the HT of $s(b)$. Ω is the energy distribution of the effective seismic signal.

The detailed derivation of (18) is attached in appendix B, which is used to obtain complex trace. Like the extraction method based on the CWT, the IF of a real-valued seismic signal is calculated via the analytical reconstructed signal shown in (18).

4. Algorithm steps to extract IF via SST-MAW

Based on the SST using the MAW, the implementation of the proposed IF estimation method can be summarized below:

(a) Apply the CWT to the seismic signal, using the MAW as the basic wavelet via equation (4);
(b) Calculate the candidate frequency of the input seismic signal by equation (15), taking use of the CWT coefficients;
(c) Relocate the wavelet transform coefficients based on the candidate frequency received via equation (16);
(d) Obtain an effective and anti-noise energy distribution of the seismic signal, taking advantage of the threshold method;
(e) Achieve the analytic reconstruction signal by equation (18);
(f) Extract the instantaneous seismic frequency via equation (3), using the reconstruction analytic signal in equation (18).

5. Numerical experiments

In this part, both synthetic and field seismic data examples are applied to test the effectiveness of the proposed method. To highlight the effectiveness and stability of the proposed approach, various IF extraction methods are also presented as comparative experiments. One is the classical HT based method. Another is the CWT approach with the common Morlet wavelet as the basic wavelet. In addition, the SST taking the Morlet wavelet as the basic wavelet is introduced as a contrast.

5.1. Synthetic data examples

Firstly, a Ricker wavelet with a dominant frequency of 30 Hz in figure 3(a) is used to verify the validity of the proposed method. The sampling frequency is 500 Hz with 500 samples. Figures 3(b)–(d) show the IFs calculated by the HT method, CWT method, and proposed approach, respectively. The three IF results are almost identical, thereby demonstrating the validity of the proposed procedure. Note that the parameters in the MAW are chosen as $\Lambda' = (3, 0.5)$ in synthetic examples.

Because seismic records are often contaminated by various kinds of noise in real applications, it is difficult to obtain the IF with high accuracy and stableness. Hence, we study how the estimated IF is impacted when there is noise in the seismic traces. Two different noise levels are tested to evaluate the noise immunity of the proposed method. Figures 4(a) and (b) depict the noisy signals contaminated by additive Gaussian white noise with SNR of 10.0 dB and 5.0 dB, respectively. The definition of the SNR is shown in equation (19)

$$\mathrm{SNR(dB)} = 10\log_{10}\left(\frac{\mathrm{var}(s(t))}{\sigma^2}\right), \tag{19}$$

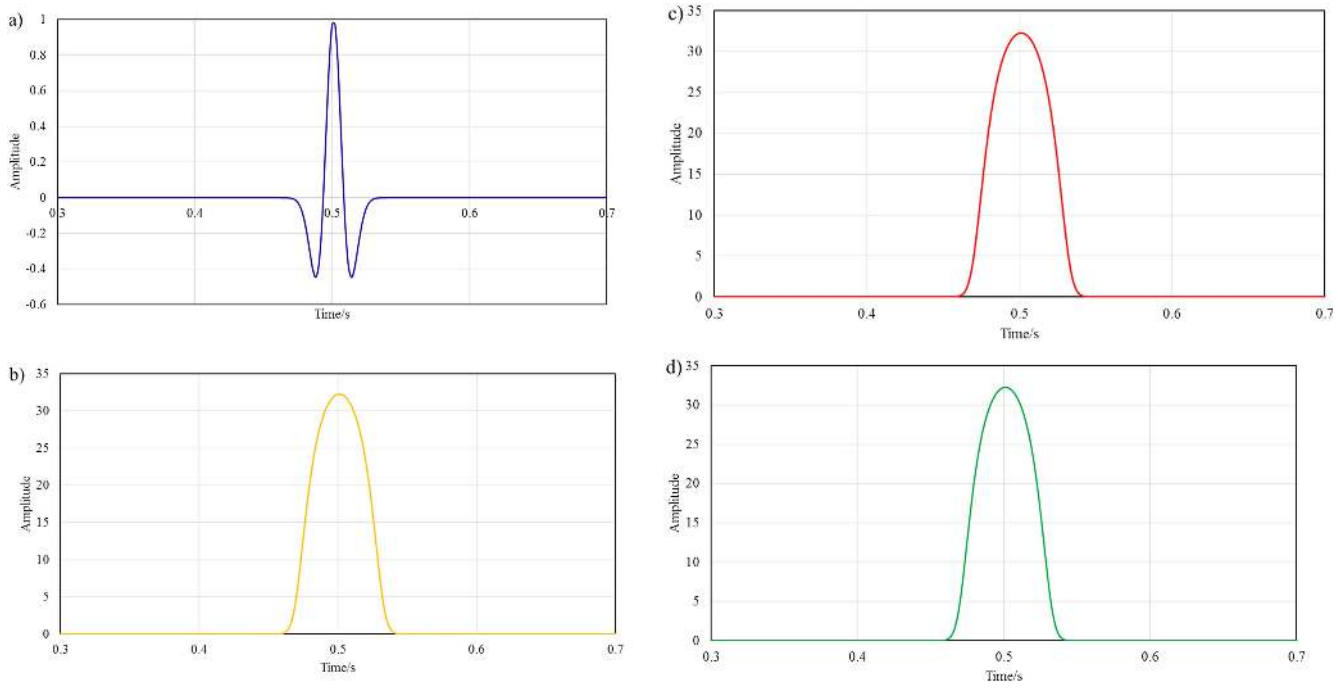

Figure 3. The test signal example. (a) The Ricker wavelet whose dominant frequency is 30 Hz, the IFs produced by the (b) HT method, (c) CWT method, and (d) proposed method.

where var($s(t)$) represents the variance of the signal $s(t)$ and σ^2 denotes the variance of the Gaussian white noise. The sample period is 4 ms, and there are 512 samples. The blue lines in the figures represent the noise-free Ricker wavelets and the red the noisy ones. Figures 4(c), (e) and (g) show the IFs calculated by the HT approach, CWT approach, and proposed approach, respectively. The blue lines represent noise-free solutions and red lines noisy. Figure 4(c) shows that the IF appears to be sensitive to the noise. The IF estimation produced by the CWT method has anti-noise performance on account of introducing the adaptive threshold in equation (6). Figure 4(g) shows that the proposed method has the most accurate and stable estimation of the IF among these three extraction results. When the SNR drops to 5.0 dB in figure 4(b), figures 4(d), (f) and (h) display the corresponding estimated results. The IF calculated by the proposed method in figure 4(h) can also give a more accurate estimation of the IF, while IF estimations obtained by the HT method and CWT method appear to be drastically degraded due to the presence of noise. It can generally be found that the proposed method can receive a more stable and precise IF estimation than the other two approaches in noisy environments.

The stability of the proposed method is evaluated further. A Ricker wavelet with coherent noise, whose SNR is about 3.0 dB, is used during the test. The bandwidth of the coherent noise is in the seismic range of about 10– 60 Hz. Figure 5(a) shows the noise-free (blue line) and noisy Ricker wavelets (red line). The sample period is 4 ms and there are 512 samples. Figure 5(b) displays spectra of noise-free data (blue line) and noisy data (red line). The IF extracted by the HT method in figure 5(c) is sensitive to the coherent noise, where the blue line represents a noise-free solution and red line noisy. Although the CWT solutions show noise immunity, the IF calculated by the proposed method in figure 5(e) gives a more accurate and stable estimation than that produced by the CWT.

5.2. Field seismic data examples

To further demonstrate the effectiveness and stability of the proposed approach, it is applied to a post-stack field 3D offshore seismic data from China National Offshore Oil Corporation. Figure 6 represents a time section of the 3D seismic data, which contains 1000 traces and 1400 ms time duration. The time sampling interval is 2 ms. According to the well data in figure 6, the sandstone reservoir is controlled by the fluvial-delta deposited system between the horizon H6 and H7 in this study area. There are many sedimentary cycles in the well log in figure 6, which can further prove that the study area is a multi-stages delta. The superimposition of sandstone bodies, indicated by the red ellipse, cannot be directly identified because this amplitude data suffers from heavy noise. Figures 7(a)–(d) show IFs obtained by the HT method, CWT method, SST taking the Morlet wavelet, and proposed method, respectively. The parameters in the MAW are chosen as $\Lambda' = (2.2,\ 0.5)$ in this filed data example. To show the superimposition of sandstone bodies clearly, we enlarge the superimposition shown in blue rectangles. Noise dramatically limits the resolution and performance of the HT method in figure 7(a). Although the CWT method reduces the influence of the noise in seismic data, the extracted IF in figure 7(b) gets

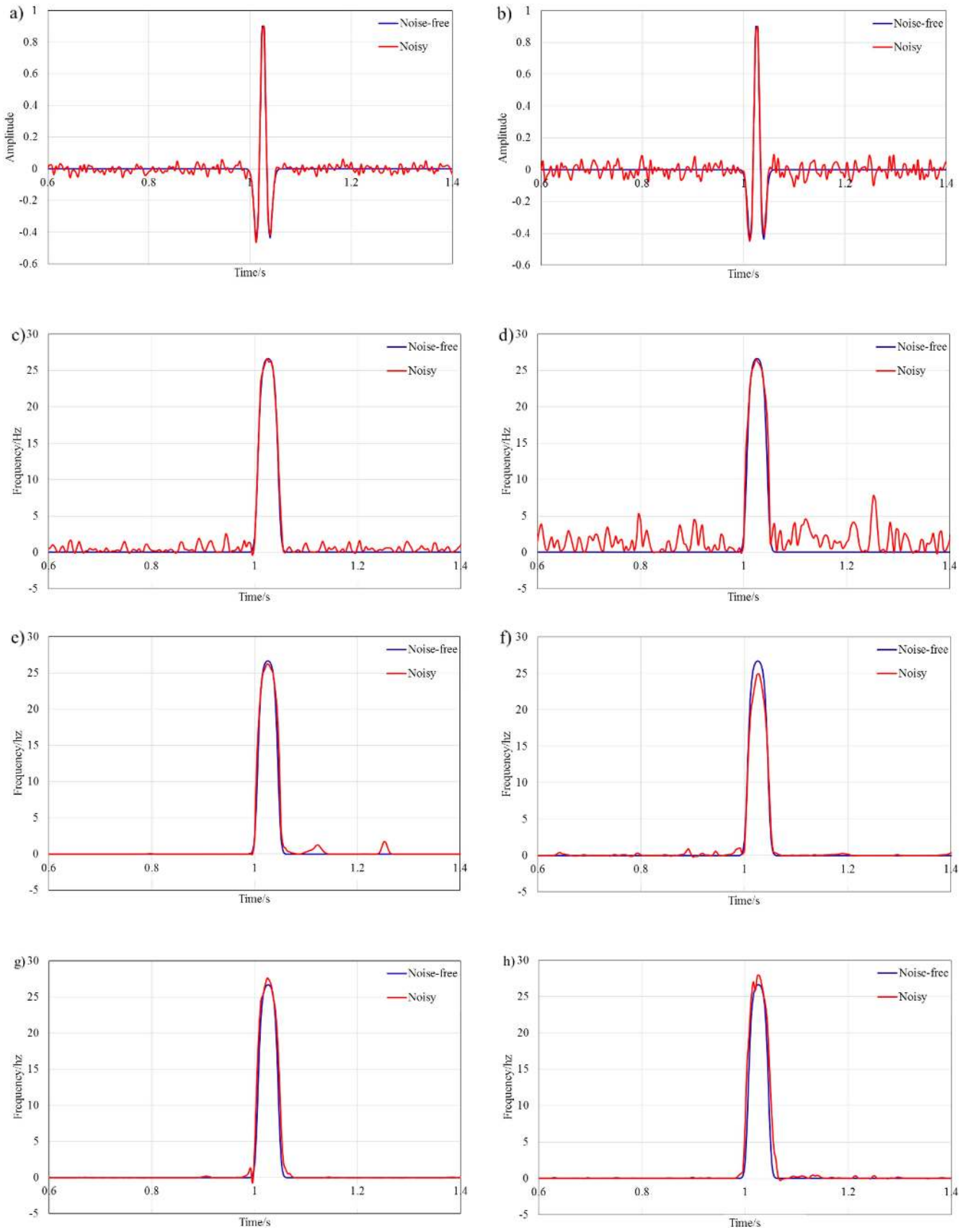

Figure 4. The noisy Ricker wavelet examples. (a) The noisy Ricker wavelet (SNR = 10.0 dB) obtained by adding Gaussian white noise to the 30 Hz Ricker wavelet, the IFs of the noisy Ricker wavelet calculated by the (c) HT method, (e) CWT method, (g) proposed method; (b) the noisy wavelet whose SNR is 5.0 dB, the corresponding estimation results are showed in (d), (f) and (h).

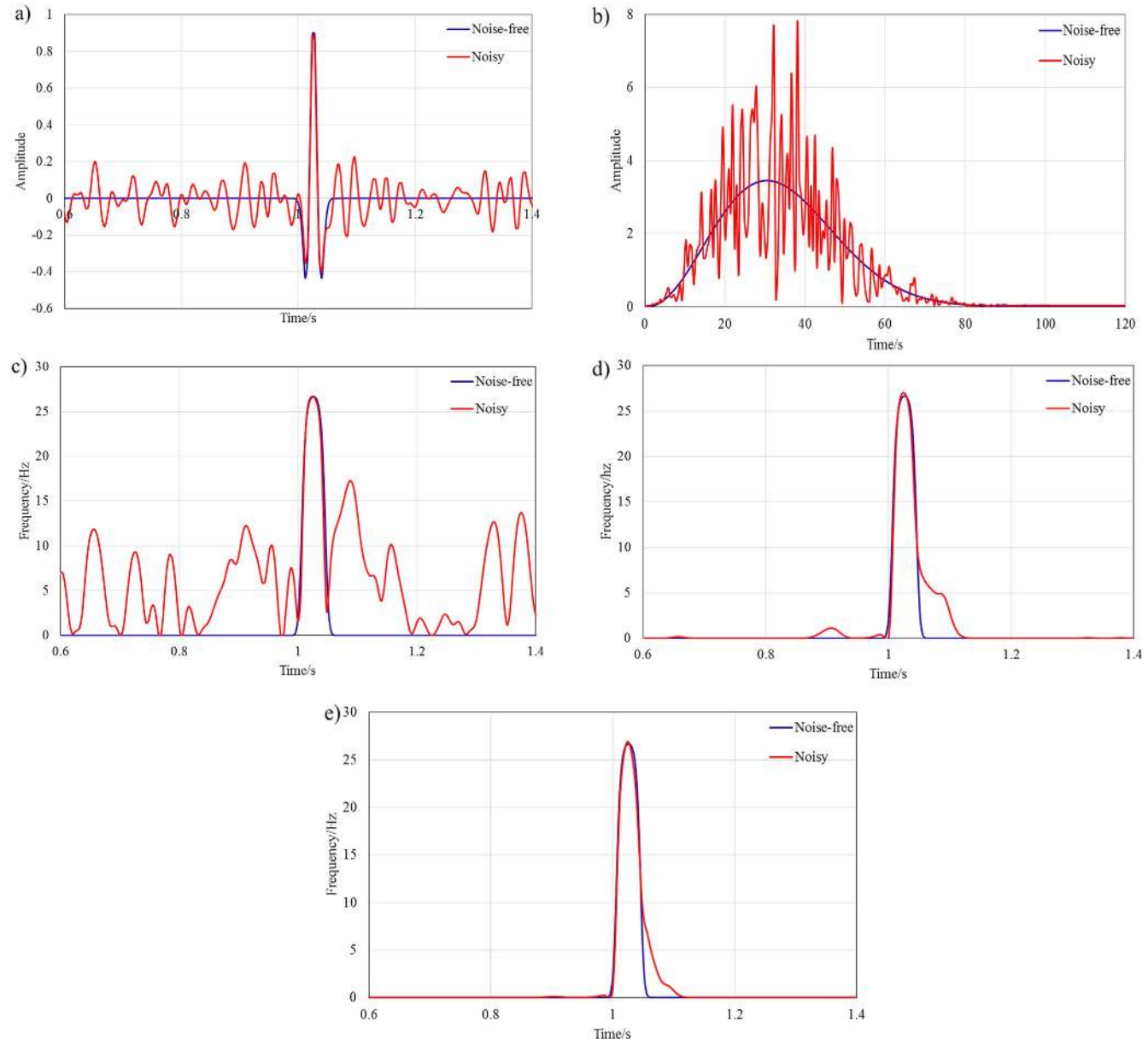

Figure 5. The noisy Ricker wavelet with coherent noise example. (a) The noise-free (blue line) and noisy (red line) Ricker wavelet with coherent noise whose SNR is 3.0 dB. The bandwidth of the coherent noise is 10–60 Hz. (b) The spectrums of the corresponding Ricker wavelets, the IFs of the Ricker wavelets calculated by the (c) HT method, (d) CWT method, (e) the proposed method. The blue lines represent noise-free solutions and red lines noisy.

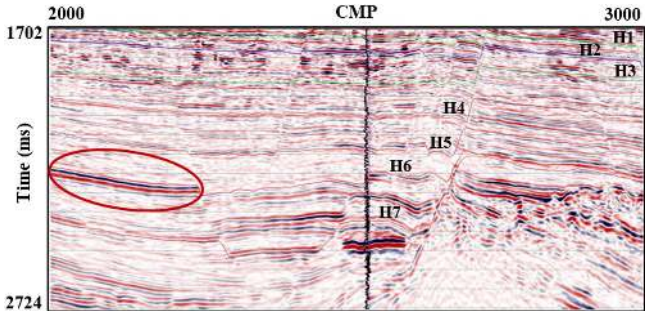

Figure 6. A seismic field section from CNOOC, which contains 1000 traces and 1400 ms time duration. The time sampling interval is 2 ms. The red ellipse indicates a stacked superimposition of sandstone bodies.

a low resolution and cannot identify stacked superimposition of sandstone bodies. The SST using the Morlet wavelet can recognize stacked sandstone bodies better, where the superimposition is much clearer than IF extractions based on the HT and CWT methods. Affected by the noise, each stacked sandstone of the SST result in figure 7(c) seems to be discrete. The last plot obtained by the proposed method shows good noise immunity. The superimposition is also the clearest of all the four plots. It can be easily concluded that the proposed method is an effective measure to identify sandstone boundaries.

The final experiment is a stacked 3D seismic data from a sedimentary basin in China, which contains many fluvial channels at different scales. The field data contains 700 inlines

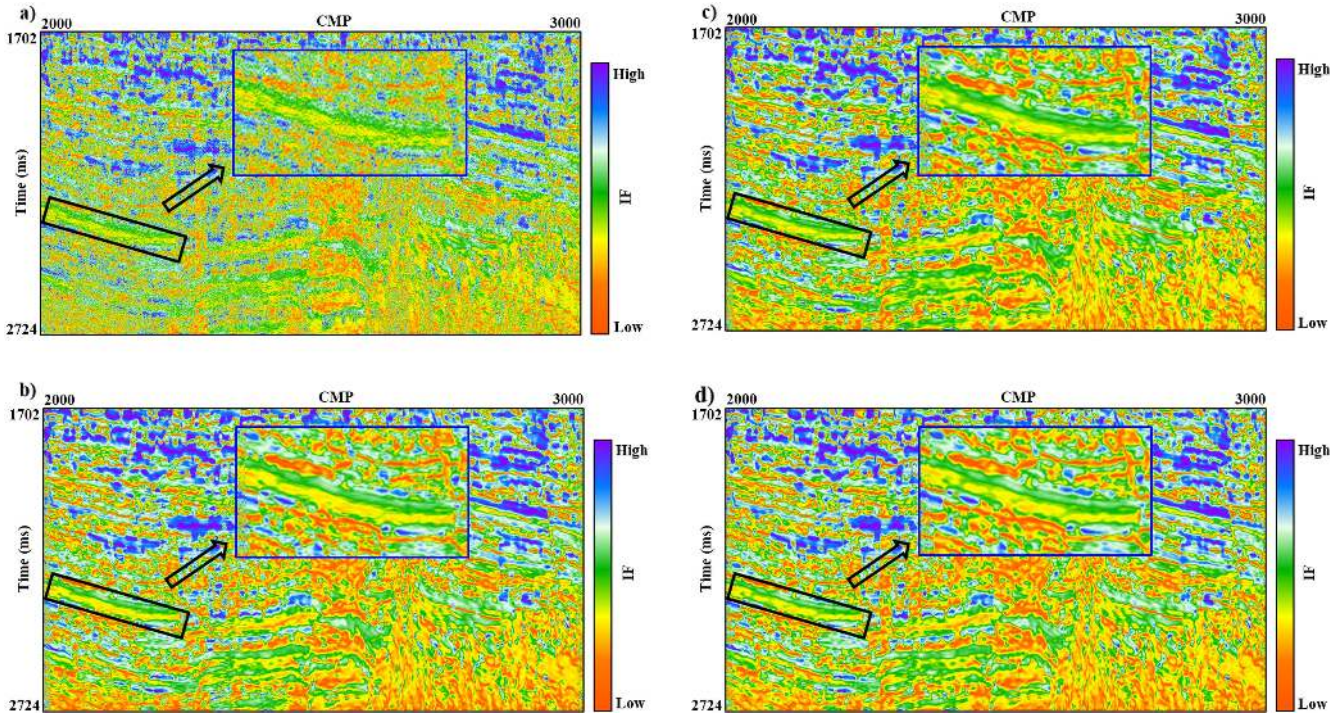

Figure 7. The IF extraction results of the seismic section shown in figure 6. The IF estimations calculated by the (a) traditional HT approach, (b) CWT approach, (c) SST taking the Morlet wavelet, (d) SST-MAW. The black rectangles identify stacked superimposition of sandstone bodies, which is enlarged in blue rectangles.

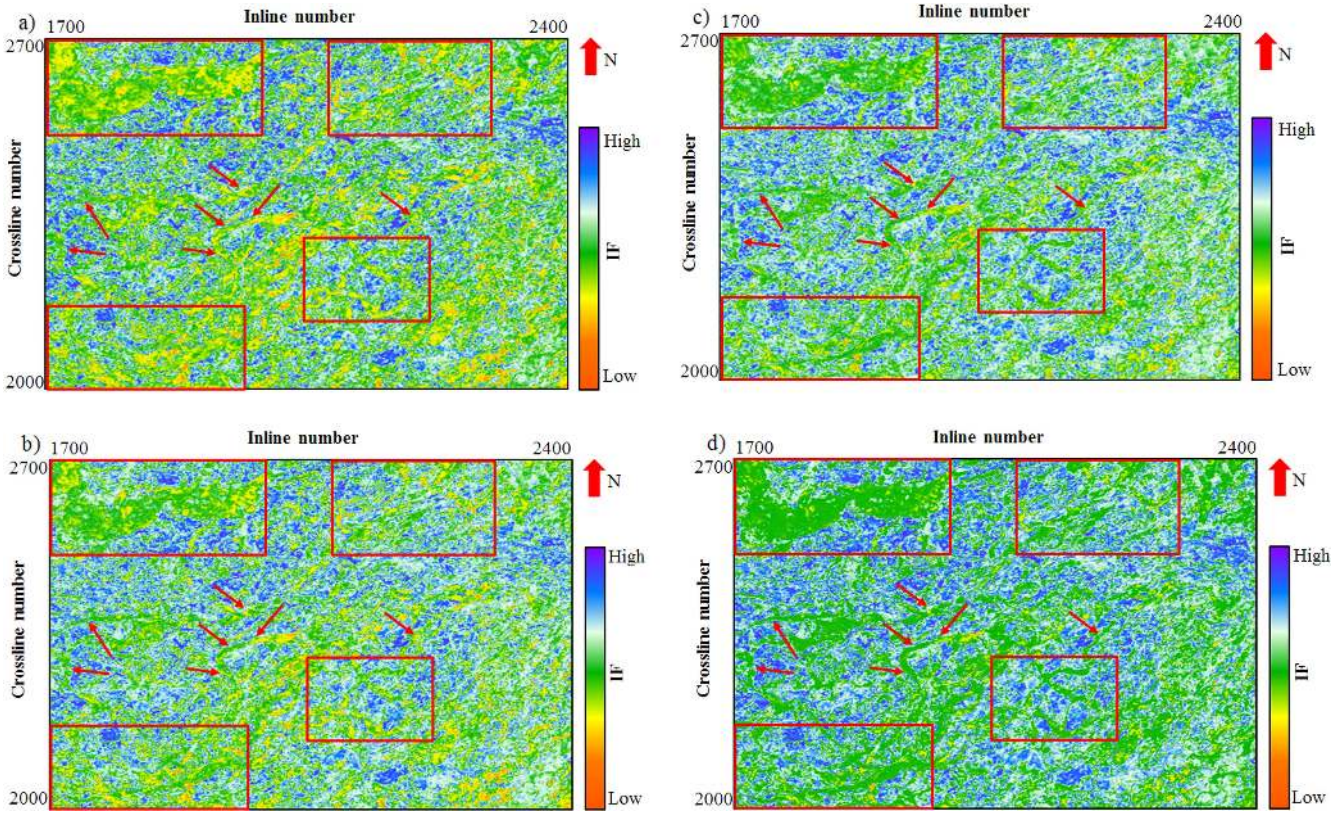

Figure 8. The 3D field data example. IF horizontal slices of a 3D stacked field seismic data calculated by (a) the HT method, (b) CWT method, (c) SST taking the Morlet wavelet and (b) the proposed approach. The channel structures at different scales are indicated by the red arrows and rectangles.

and 700 crosslines. The IF data cubes are calculated by the HT method, CWT method, SST-Morlet, and SST-MAW. Then, horizontal slices of the IF data cubes are extracted, shown in figure 8. In this experiment, the frequency axes are scaled with numbers from 10 to 70. It can be seen that the characterization of channels is unclear because the HT method suffers from noise heavily. The IF extractions, produced by the CWT method and SST taking the Morlet wavelet, show anti-noise performance, but the channels are not distinct enough to distinguish. On account of the anti-noise performance and the high resolution, the proposed method gets a stable and anti-noise IF, which can reveal distinct and continuous subtle channel features at different scales (indicated by the red arrows and rectangles). The proposed method describes the edges of channels at different scales much clearly than the other three methods. This illustrates geological features can be characterized with high resolution by introducing the proposed approach to seismic data analysis.

6. Conclusions

We have introduced a method to estimate instantaneous seismic frequency (IF), based on the SST taking the MAW. The MAW can help improve time–frequency resolution by matching seismic wavelets well, which is an analytic wavelet and comes from the TPW. The SST can create a robust and sparse time–frequency representation by squeezing values along its frequency axis. Using the MAW as the basic wavelet in the SST-MAW, we can reconstruct a complex signal to extract instantaneous seismic frequency. The IF estimated by the SST-MAW is robust to noisy data and yields improved accuracy. The results on synthetic signals show the advantages of the proposed procedure in both resolution and anti-noise performance by comparing with the HT based method, CWT based approach, and some other comparative methods. After applying the proposed approach to 2D and 3D field data, we can easily characterize geological structures (such as the channels) with high resolution and precision. We can conclude that the proposed IF extraction method has the potential to identify sandstone boundary and fluvial channel features with high resolution under noise contamination, which is helpful to seismic data interpretation and further oil/gas reservoir identification.

Acknowledgments

This work is partially funded by the Major National Science and Technology Projects (2016ZX05024-001-007 and 2017ZX050609) and the National Natural Science Foundation of China (41390454, 41390454 and 61501366). We appreciate Eugene Brevdo for his MATLAB Synchrosqueezing Toolbox (https://web.math.princeton.edu/~ebrevdo/synsq/). We also want to thank Professors Bo Zhang and Jing Ba, Dr Hui Li and Dr Qingbao Zhou for their fruitful discussions about this work. We would like to acknowledge the editor and reviewers for their comments and suggestions, which helped to improve the paper.

Appendix A. Parameter selection in the MAW

Choosing a matching wavelet in the CWT, we can achieve a time–frequency representation with high resolution. The MAW matches the Ricker wavelet better than the popular Morlet wavelet, which has been proved in figure 2. There are two parameters in the MAW. Choosing appropriate σ and τ in the MAW, we can make the MAW in equation (12) match the Ricker wavelet to improve the time–frequency resolution of the CWT.

In this paper, the two parameters in the MAW can be optimized and chosen based on the concentration measure (CM) approach (Jones and Parks 1990, Sejdić *et al* 2008), which is designed to minimize the energy concentration for any time–frequency representation based on the automatic determination of some time–frequency distribution parameters (Stanković 2001). Introducing the CM method, the parameters in the MAW can be chosen as the following steps:

(1) For each selected from the given set $\{(\sigma, \tau)\}$, calculate the CWT-MAW $S(b, a)$ taking used of equation (13).

(2) For each (σ, τ) in the given set, normalize the energy of the CWT coefficients, so that all of the representations with different (σ, τ) have the equal energy as

$$\overline{S^{(\sigma,\tau)}(b, a)} = \frac{S^{(\sigma,\tau)}(b, a)}{\sqrt{\int_{-\infty}^{\infty}\int_{-\infty}^{\infty}|S^{(\sigma,\tau)}(b, a)|^2 \mathrm{d}b\mathrm{d}a}}. \tag{A1}$$

(3) For each (σ, τ) in the given set, calculate the CM as

$$CM(\sigma, \tau) = \left[\int_{-\infty}^{\infty}\int_{-\infty}^{\infty}|\overline{S^{(\sigma,\tau)}(b, a)}|^{\frac{1}{p}}\,\mathrm{d}b\mathrm{d}a\right]^p, \tag{A2}$$

where p is chosen as 3 in this paper (Jones and Parks 1990, Stanković 2001).

(4) By the following equation, we can determine the optimal parameters $(\sigma, \tau)_{\mathrm{opt}}$.

$$(\sigma, \tau)_{\mathrm{opt}} = \min_{(\sigma,\tau)}[\mathrm{CM}(\sigma, \tau)]. \tag{A3}$$

(5) Based on the $(\sigma, \tau)_{\mathrm{opt}}$ in equation (A3), define the optimal CWT-TPW coefficients as

$$S^{\mathrm{opt}}(b, a) = S^{(\sigma,\tau)_{\mathrm{opt}}}(b, a). \tag{A4}$$

Note that the proposed method calculates the CWT-MAW for each (σ, τ) in the given set $\{(\sigma, \tau)|0 < \sigma < 5,\ 0 < \tau < 1\}$. Based on the computed CWT coefficients, we can calculate the $\mathrm{CM}(\sigma, \tau)$ for each (σ, τ). The minimum of the CM corresponds the optimized $(\sigma, \tau)_{\mathrm{opt}}$, which provides the least smear of $S^{\mathrm{opt}}(b, a)$.

Appendix B. Proof of equation (18)

$\psi_{\mathrm{mod}}(t; \Lambda')$ is an analytic wavelet with its real part $\psi_{\mathrm{mod}\,-R}(t; \Lambda')$ being even and $C_{\psi_{\mathrm{mod}}} = \int_0^{\infty}(\hat{\psi}_{\mathrm{mod}\,-R}(\omega; \Lambda')/\omega)\mathrm{d}\omega$, with $0 <$

$C_\psi < \infty$. And $\hat{\psi}_{\mathrm{mod}}(\omega;\Lambda') = \int_{-\infty}^{\infty} \psi_{\mathrm{mod}}(t;\Lambda')\mathrm{e}^{-\mathrm{i}\omega t}\mathrm{d}t$ is the Fourier transform of the basic wavelet. Then for an arbitrary real $s(t) \in L^2(R, \mathrm{d}t)$, we have (Gao *et al* 1999)

$$\begin{aligned} S(b,a) &= \int_{-\infty}^{\infty} a^{-1}s(t)\overline{\psi_{\mathrm{mod}}\left(\frac{t-b}{a};\Lambda'\right)}dt, \\ &= \int_{-\infty}^{\infty} a^{-1}s(t)\left[\psi_{\mathrm{mod}-R}\left(\frac{t-b}{a};\Lambda'\right)\right. \\ &\quad \left. -\mathrm{i}\psi_{\mathrm{mod}-I}\left(\frac{t-b}{a};\Lambda'\right)\right]\mathrm{d}t, \\ &= \int_{-\infty}^{\infty} a^{-1}s(t)\psi_{\mathrm{mod}-R}\left(\frac{t-b}{a};\Lambda'\right)\mathrm{d}t \\ &\quad -\mathrm{i}\int_{-\infty}^{\infty} a^{-1}s(t)\psi_{\mathrm{mod}-I}\left(\frac{t-b}{a};\Lambda'\right)\mathrm{d}t \\ &= S_R(b,a) + \mathrm{i}S_I(b,a), \end{aligned} \tag{B1}$$

where

$$\begin{aligned} &\psi_{\mathrm{mod}-R}(t;\Lambda') = \mathrm{Re}(\psi_{\mathrm{mod}}(t;\Lambda')), \\ &\psi_{\mathrm{mod}-I}(t;\Lambda') = \mathrm{Im}(\psi_{\mathrm{mod}}(t;\Lambda')), \\ &S_R(b,a) = \int_{-\infty}^{\infty} a^{-1}s(t)\psi_{\mathrm{mod}-R}\left(\frac{t-b}{a};\Lambda'\right)\mathrm{d}t, \\ &S_I(b,a) = -\int_{-\infty}^{\infty} a^{-1}s(t)\psi_{\mathrm{mod}-I}\left(\frac{t-b}{a};\Lambda'\right)\mathrm{d}t. \end{aligned}$$

and then in SST, we can obtain

$$\begin{aligned} T(\omega,b) &= \int_A S(a,b)a^{-1}\mathrm{d}a, \\ &= \int_A [S_R(a,b) + \mathrm{i}S_I(a,b)]a^{-1}\mathrm{d}a, \\ &= \int_A S_R(a,b)a^{-1}\mathrm{d}a + \mathrm{i}\int_A S_I(a,b)a^{-1}\mathrm{d}a, \\ &= T_R(\omega,b) + \mathrm{i}T_I(\omega,b), \end{aligned} \tag{B2}$$

where $A = \{a > 0 | \omega_s(a,b) = \omega, S(a,b) \neq 0\}$,

$T_R(\omega,b) = \int_A S_R(a,b)a^{-1}\mathrm{d}a$ and $T_I(\omega,b) = \int_A S_I(a,b)a^{-1}\mathrm{d}a$.

Both sides of (B2) multiplied by $1/C_{\psi_{\mathrm{mod}}}$ and then integrate it concerning ω from zero to infinity

$$\begin{aligned} \frac{1}{C_\psi}\int_0^\infty T(\omega,b)\mathrm{d}\omega &= \frac{1}{C_\psi}\int_0^\infty [T_R(\omega,b) + \mathrm{i}T_I(\omega,b)]\mathrm{d}\omega, \\ &= s(b) + \mathrm{i}H[s(b)]. \end{aligned} \tag{B3}$$

When ω is discrete as the body of the context, we can get the discrete form of (B3) as follows

$$s(b) + \mathrm{i}H[s(b)] = \frac{1}{C_{\psi_{\mathrm{mod}}}}\sum_{l,\Omega} T_s(\omega_l,b)(\Delta\omega), \tag{B4}$$

where $H[s(b)]$ is the HT of $s(b)$. Ω is the energy distribution of the effective seismic signal. (B4) is (18) in the body of the context.

Based on the above consequences, the analytic counterpart of a field valued signal can be calculated with its synchrosqueezing coefficients, and the IF can be estimated using equations (3) and (B4).

References

Barnes A E 1993 Instantaneous spectral bandwidth and dominant frequency with applications to seismic reflection data *Geophysics* **58** 419–28

Barnes A E 2007 A tutorial on complex seismic trace analysis *Geophysics* **72** W33–43

Brevdo E, Fuckar N, Thakur G and Wu H 2013 The synchrosqueezing algorithm: a robust analysis tool for signals with time-varying spectrum *Signal Process.* **93** 1079–94

Burg J P 1975 Maximum entropy spectrum analysis *PhD Thesis* Stanford University

Chopra S and Marfurt K J 2005 Seismic attributes—a historical perspective *Geophysics* **70** 3SO–8SO

Cohen L 1995 *Time-Frequency Analysis* (Englewood Cliffs ,NJ: Prentice-Hall PTR)

Daubechies I, Lu J and Wu H 2011 Synchrosqueezed wavelet transform: an empirical mode decomposition-like tool *Appl. Comput. Harmon. Anal.* **30** 243–61

Donoho D L 1995 De-noising by soft-thresholding *IEEE Trans. Inf. Theory* **41** 613–27

Fomel S 2007 Local seismic attributes *Geophysics* **72** A29–33

Guo H, Lewis S and Marfurt K J 2008 Mapping multiple attributes to three- and four-component color models—a tutorial *Geophysics* **73** W7–19

Gao J H, Dong X, Wang W, Li Y and Pan C 1999 Instantaneous parameters extraction via wavelet transform *IEEE Trans. Geosci. Remote Sens.* **37** 867–70

Gao J H, Wan T, Chen W and Mao J 2006 Three parameter wavelet and its applications to seismic data processing *Chin. J. Geophys.-CH* **49** 1802–12

Gao J H, Wang W and Zhu G 1996 On the choice of wavelet functions for seismic data processing *Chin. J. Geophys.-CH* **39** 400–7

Hahn L S 1996 *Hilbert Transform in Signal Process* (London: Artech House)

Harrop J D, Taraskin S and Eiiiott S 2002 Instantaneous frequency and amplitude identification using wavelets: application to glass structure *Phys. Rev.* E **66** 026703

Herrera R H, Han J and van der Baan M 2014 Applications of the synchrosqueezing transform in seismic time-frequency analysis *Geophysics* **79** 55–64

Holschneider M and Kon M 1996 *Wavelets: An Analysis Tool* (Oxford: Oxford University Press)

Huang N E and Wu Z 2008 A review on Hilbert–Huang transform: method and its applications to geophysical studies *Rev. Geophys.* **46** 1–23

Jones D L and Parks T W 1990 A high resolution data-adaptive time-frequency representation *IEEE Trans. Signal Process.* **38** 2127–36

Kourki M and Riahi M A 2014 Seismic facies analysis from pre-stack data using self-organizing maps *J. Geophys. Eng.* **11** 065005

Li X F, Wen C and Zhou Y 2014 The instantaneous frequency estimation based on ensemble empirical mode decomposition *J. Appl. Geophys.* **111** 102–9

Lilly J M and Olhede S 2010 On the analytic wavelet transform *IEEE Trans. Inf. Theory* **56** 4135–56

Lilly J M and Olhede S 2012 Generalized Morse wavelets as a superfamily of analytic wavelets *IEEE Trans. Signal Process.* **60** 6036–41

Mandel L 1974 Interpretation of instantaneous frequencies *Am. J. Phys.* **42** 840–6

Marfurt K J, Kirlin R, Farmer S and Bahorich M 1998 3D seismic attributes using a semblance-based coherency algorithm *Geophysics* **63** 1150–65

Olhede S C and Walden A 2002 Generalized Morse wavelets *IEEE Trans. Signal Process.* **50** 2661–70

Sejdi E, Djurovi I and Jiang J 2008 A window width optimized S-transform *EURASIP J. Adv. Signal Process.* **59** 672941

Stanković L J 2001 A measure of some time-frequency distributions concentration *Signal Process.* **81** 621–31
Taner M T, Foehler K and Sheriff R 1979 Complex seismic trace analysis *Geophysics* **44** 1041–63
Torrence C and Compo G 1998 A practical guide to wavelet analysis *Bull. Am. Meteorol. Soc.* **79** 61–78
Wang P and Gao J 2013 Extraction of instantaneous frequency from seismic data via the generalized Morse wavelets *J. Appl. Geophys.* **93** 83–92
Wang P, Gao J and Wang Z 2014 Time-frequency analysis of seismic data using synchrosqueezing transforms *IEEE Geosci. Remote Sens. Lett.* **11** 2042–4
Wang Z G, Gao J, Zhou Q, Li K and Peng J 2013 A new extension of seismic instantaneous frequency using a fractional time derivative *J. Appl. Geophys.* **98** 176–81
White R E 1991 Properties of instantaneous seismic attributes *Leading Edge* **10** 26–32
Yang S L and Gao J 2010 Seismic attenuation estimation from instantaneous frequency *IEEE Geosci. Remote Sens. Lett.* **7** 113–7
Zeng H L 2010 Geologic significance of anomalous instantaneous frequency *Geophysics* **75** P23–30
Zoukaneri I and Porsani M 2015 A combined Wigner–Ville and maximum entropy method for high-resolution time-frequency analysis of seismic data *Geophysics* **80** O1–11